LETTER

doi:10.1038/nature19813

Evolution of *Hoxa11* regulation in vertebrates is linked to the pentadactyl state

Yacine Kherdjemil[1,2], Robert L. Lalonde[3], Rushikesh Sheth[1], Annie Dumouchel[1], Gemma de Martino[1]†, Kyriel M. Pineault[4], Deneen M. Wellik[4], H. Scott Stadler[5], Marie-Andrée Akimenko[3] & Marie Kmita[1,2,6]

The fin-to-limb transition represents one of the major vertebrate morphological innovations associated with the transition from aquatic to terrestrial life and is an attractive model for gaining insights into the mechanisms of morphological diversity between species[1]. One of the characteristic features of limbs is the presence of digits at their extremities. Although most tetrapods have limbs with five digits (pentadactyl limbs), palaeontological data indicate that digits emerged in lobed fins of early tetrapods, which were polydactylous[2]. How the transition to pentadactyl limbs occurred remains unclear. Here we show that the mutually exclusive expression of the mouse genes *Hoxa11* and *Hoxa13*, which were previously proposed to be involved in the origin of the tetrapod limb[1–6], is required for the pentadactyl state. We further demonstrate that the exclusion of *Hoxa11* from the *Hoxa13* domain relies on an enhancer that drives antisense transcription at the *Hoxa11* locus after activation by HOXA13 and HOXD13. Finally, we show that the enhancer that drives antisense transcription of the mouse *Hoxa11* gene is absent in zebrafish, which, together with the largely overlapping expression of *hoxa11* and *hoxa13* genes reported in fish[3–7], suggests that this enhancer emerged in the course of the fin-to-limb transition. On the basis of the polydactyly that we observed after expression of *Hoxa11* in distal limbs, we propose that the evolution of *Hoxa11* regulation contributed to the transition from polydactyl limbs in stem-group tetrapods to pentadactyl limbs in extant tetrapods.

Several studies provided evidence for the implication of Hox genes in the fin-to-limb transition[8–13], notably *Hoxa13* and *Hoxd13* (*Hox13* hereafter), which are required for digit morphogenesis[10–14]. Comparison of their expression pattern in fin and limb buds revealed a significant expansion of the *Hox13* domain in distal limbs[15] and engineered enlargement of the *Hoxd13* domain in fish resulted in more chondrogenic tissue forming distally as well as fin fold reduction[12]—that is, morphological changes associated with the fin-to-limb transition. It was thus proposed that the evolution of *Hox13* regulation has likely been instrumental to the emergence of the limb characteristic feature, that is, the digits[10,12]. In mice, this regulation relies on a series of remote transcriptional enhancers[16,17], and although a subset of these enhancers exists in fish[18], the expansion of the *Hox13* domain in limb was probably associated with the emergence of tetrapod-specific enhancers during the fin-to-limb transition[10–13]. Another notable difference is the mutually exclusive expression of *Hoxa11* and *Hoxa13* in tetrapod limbs, contrasting with their largely overlapping expression in fins[3–7]. Two hypotheses have been put forward to explain how *Hoxa11* gets proximally restricted in tetrapod limbs. One hypothesis suggested a *Hoxa13*-dependent repression of *Hoxa11* in the presumptive autopod[9,13,19], whereas the second proposed that antisense transcription at the *Hoxa11* locus prevents expression of the gene distally[20–22], but the functional importance of the mutually exclusive expression of *Hoxa11* and *Hoxa13* in tetrapod limbs is unknown.

Previous chromatin conformation analyses revealed that, in distal limbs, 5′ *HoxA* genes (that is, *Hoxa9* to *Hoxa13*) are grouped within a chromatin sub-topological domain (sub-TAD) interacting with sub-TADs containing distal limb enhancers[17]. Yet, although *Hoxa10* and *Hoxa13* are both expressed distally, *Hoxa11* expression is proximally restricted (Fig. 1a–c), suggesting that *Hoxa11* is part of the distal limb regulatory landscape, but a specific, yet unknown, mechanism prevents its expression distally[13,19]. To test this possibility, we first took advantage of a mouse line in which the *Hoxa11* gene is replaced by a PGK-neomycin resistance cassette[23], which we used as a reporter transgene. We found neomycin expression in distal limbs (Fig. 1d), indicating that *Hoxa11* proximal restriction is linked to specific feature(s) of the gene itself. We next analysed the putative implication of antisense long non-coding RNAs previously identified at the *Hoxa11* locus[20,21] and robustly expressed in the distal limb bud[20] (Fig. 1e). Among the distinct *Hoxa11* antisense transcripts (*Hoxa11as*, also known as *Hoxa11os*), two initiate upstream of the *Hoxa11* gene and are thus non-overlapping with *Hoxa11* (*Hoxa11as-a*; Fig. 1e) and the other two initiate within *Hoxa11* exon 1 (*Hoxa11as-b*; Fig. 1f). Notably, only *Hoxa11as-b* expression pattern is mutually exclusive with *Hoxa11* expression domain (Fig. 1f, compare with Fig. 1b). To test whether antisense transcription overlapping with *Hoxa11* exon 1 prevents *Hoxa11* expression distally, we took advantage of the $Hoxa11^{eGFP}$ mutant line, which lacks *Hoxa11as-b* start sites as the enhanced green fluorescent protein (eGFP) coding sequence replaces most of *Hoxa11* exon 1 (ref. 24). This mutation disrupted antisense transcription normally initiating 3′ to *Hoxa11* promoter (Extended Data Fig. 1a, b) while *gfp* expression driven by the *Hoxa11* promoter was present both in the proximal and distal domains (Fig. 1g). By contrast, ectopic expression of *Hoxa11as-b* in the entire limb had no effect on *Hoxa11* expression (Extended Data Fig. 2c–e), thereby excluding a *trans*-acting effect of *Hoxa11as-b* on *Hoxa11* expression. Together, our data suggest that *Hoxa11* distal repression is due to the antisense transcription event or the antisense *Hoxa11as-b* transcripts acting in *cis*.

Previous mapping of active enhancers in distal limbs[17] (referred to as 'digit' enhancers hereafter) uncovered a putative 'digit' enhancer embedded in *Hoxa11* intron. We thus proposed that this enhancer might control *Hoxa11as-b* expression. We first tested the transcriptional enhancer activity of this DNA region in transgenic embryos and confirmed its ability to act as a transcriptional enhancer in distal limbs (Fig. 2a). Next, we generated mutant mice lacking this enhancer ($Hoxa11^{\Delta Int/\Delta Int}$; Extended Data Fig. 2) to examine its potential implication in *Hoxa11as-b* expression. Analysis of antisense transcription in $Hoxa11^{\Delta Int/\Delta Int}$ limbs showed no detectable expression of *Hoxa11as-b* in the most distal cells (Fig. 2b, c), indicating that in these cells, the

[1]Genetics and Development Research Unit, Institut de Recherches Cliniques de Montréal, Montréal, Québec H2W 1R7, Canada. [2]Département de Médecine (Programme de Biologie Moléculaire), Université de Montréal, Montréal, Québec H3T 1J4, Canada. [3]Department of Biology and CAREG, University of Ottawa, Ottawa, Ontario K1N 6N5, Canada. [4]Department of Internal Medicine, Division of Molecular Medicine and Genetics, University of Michigan, Ann Arbor, Michigan 48109-2200, USA. [5]Shriners Hospital for Children, Portland, Oregon 97239, USA. [6]Department of Experimental Medicine, McGill University, Montreal, Quebec H3A 1A3, Canada. †Present address: Department of Biology, McGill University, Montreal, Quebec H3A 1B1, Canada.

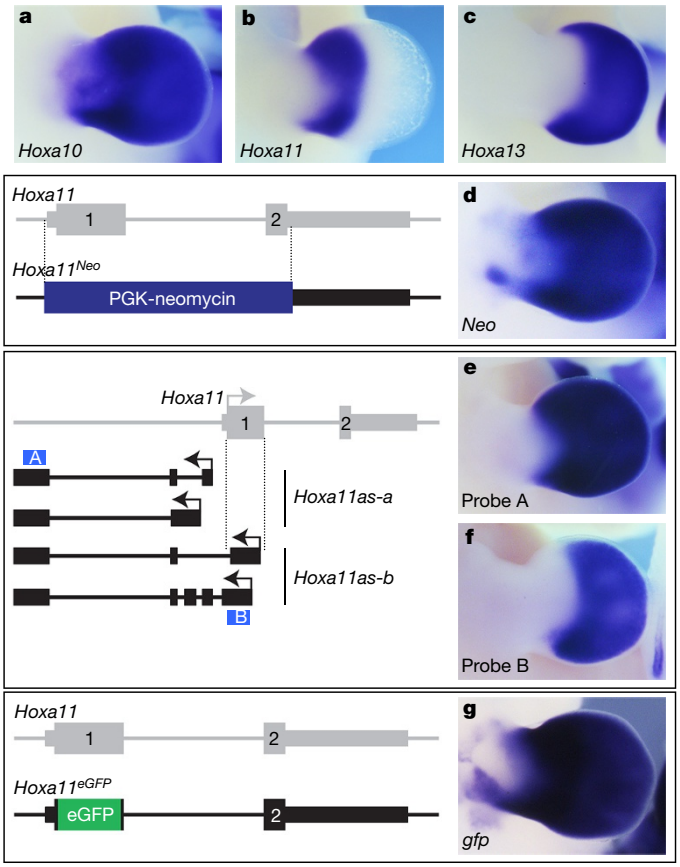

Figure 1 | The proximal restriction of *Hoxa11* is linked to antisense transcription at the *Hoxa11* locus. a–c, Expression of *Hoxa10* (**a**), *Hoxa11* (**b**) and *Hoxa13* (**c**) in wild-type limb bud from embryonic day (E) 11.5 mouse. **d**, Replacement of the *Hoxa11* gene with the PGK-neomycin cassette (*Hoxa11*^{Neo}; scheme to the left), results in neomycin expression both in the proximal and distal domains. **e**, **f**, Expression of all antisense transcripts (**e**) and antisense transcripts overlapping with *Hoxa11* exon 1 (**f**) in E11.5 wild-type limb. Schemes of the antisense transcripts and the probes used (blue boxes) are on the left. Note that the antisense transcripts overlapping with *Hoxa11* exon 1 (*Hoxa11as-b*) are distally restricted (**f**), reminiscent of *Hoxa13* expression (**c**) and mutually exclusive with the *Hoxa11* pattern (**b**). **g**, Deletion of the antisense transcript start sites in *Hoxa11* exon 1, via replacement of most of exon 1 with the eGFP coding sequence (*Hoxa11*^{eGFP}; scheme to the left) and expression of *gfp* under the control of the *Hoxa11* promoter (right). Original magnification, ×31.5 (for all images).

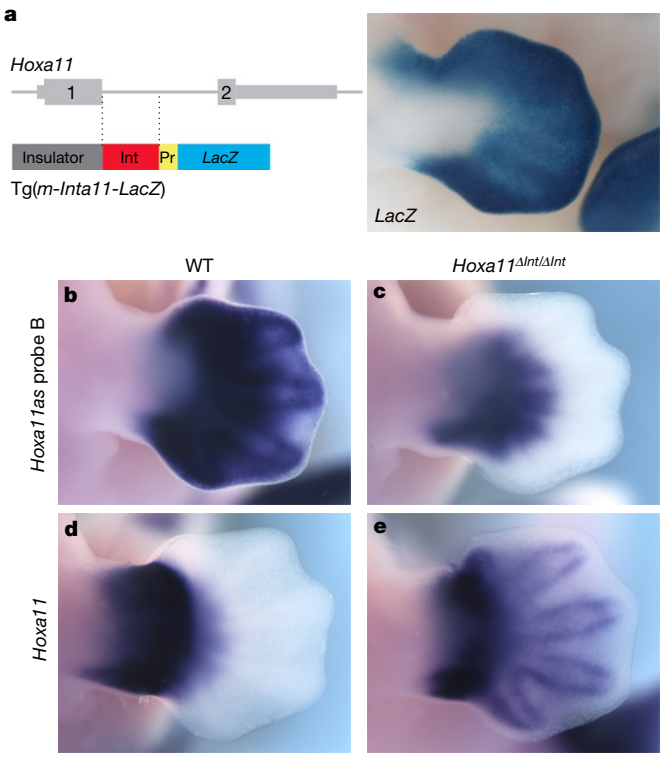

Figure 2 | Deletion of the distal enhancer in *Hoxa11* intron results in impaired antisense transcription and gain of sense transcription in distal cells. a, Left, scheme of the Tg(*m-Inta11-LacZ*) transgene carrying the predicted distal enhancer (Int, red box). Right, X-gal staining of E12.5 transgenic embryos ($n = 5$). **b–e**, Expression of *Hoxa11as-b* (**b**, **c**) and *Hoxa11* (**d**, **e**) in wild-type (WT; **b**, **d**) and *Hoxa11*$^{\Delta Int/\Delta Int}$ (**c**, **e**) mouse limbs at E12.5. Note that based on the observed gain of *Hoxa11* expression, other regulatory input(s) could be implicated in *Hoxa11* regulation in distal cells. Pr, minimal promoter. Original magnification, ×31.5 (for all images).

identified enhancer is required for antisense transcription overlapping with *Hoxa11* exon 1. Some *Hoxa11as-b* expression remained in proximal cells of the presumptive handplate (presumptive carpal region; Fig. 2c), which suggests that additional *cis*-regulatory element(s) trigger antisense transcription in these cells. Notably, the deletion of the enhancer abrogating *Hoxa11as-b* expression in the most distal cells also resulted in ectopic expression of *Hoxa11* in the presumptive digits (Fig. 2d, e). The gain-of-sense transcription in *Hoxa11*$^{eGFP/eGFP}$ distal limbs (Fig. 1g) indicates that it is not the intronic regulatory region per se but *Hoxa11as-b* expression or the antisense transcription event that represses *Hoxa11* expression distally.

Analysis of the enhancer sequence revealed several putative binding sites for HOXA13, the expression of which occurs in digit progenitor cells[25] and is required in conjunction with HOXD13 for digit morphogenesis[14]. Chromatin immunoprecipitation followed by high-throughput sequencing (ChIP–seq) indicated that, in distal limb cells, HOXA13 as well as HOXD13 bind to the identified enhancer (Extended Data Fig. 3a). Moreover, transcription assay in 293T cells shows that HOXA13 has a positive effect on the enhancer activity (Extended Data Fig. 3b). Together, these results raised the possibility that distal *Hoxa11* antisense transcription relies on HOX13. We thus analysed *Hoxa11* antisense transcription in the *Hoxa13;Hoxd13* allelic series. We used the probe recognizing all antisense transcripts such that expression in the proximal limb, where *Hox13* genes are not expressed, served as internal control. We found that although antisense transcription is barely modified in single mutants (Extended Data Fig. 4), it markedly decreases in the *Hoxa13*$^{-/-}$ *Hoxd13*$^{+/-}$ mutant (Fig. 3c, compare to Fig. 3a), and is completely abrogated in *Hoxa13*$^{-/-}$ *Hoxd13*$^{-/-}$ distal limbs (Fig. 3e). Analysis of the distal-specific antisense transcripts (*Hoxa11as-b)* confirmed that distal antisense transcription requires HOX13 function (Extended Data Fig. 5). Importantly, concomitant with the abrogation of antisense transcription, *Hoxa11* expression was gained distally (Fig. 3d–f, compare with Fig. 3b) consistent with the requirement of antisense transcription for *Hoxa11* proximal restriction.

To assess the functional significance of the HOXA13/D13-mediated repression of *Hoxa11*, we investigated the phenotypic outcome of distal *Hoxa11* expression. Although the deletion of the enhancer driving antisense transcription results in *Hoxa11* expression in distal limbs, the deletion extends up to the exon 1–intron boundary, thereby precluding the use of this mutant line to assess the phenotype resulting from distal *Hoxa11* expression. We thus generated a *Hoxa11* conditional gain-of-function allele (*Rosa26*^{Hoxa11}; Extended Data Fig. 6) to express *Hoxa11* ectopically and distally. We found that embryos carrying the *Rosa26*^{Hoxa11} allele and either *Hoxa13:Cre* (ref. 25) or *Prx1:Cre* (ref. 26) have limbs with extra digits (Fig. 3g, h), including postaxial extra digits (arrow in Fig. 3h and Extended Data Fig. 7). While some

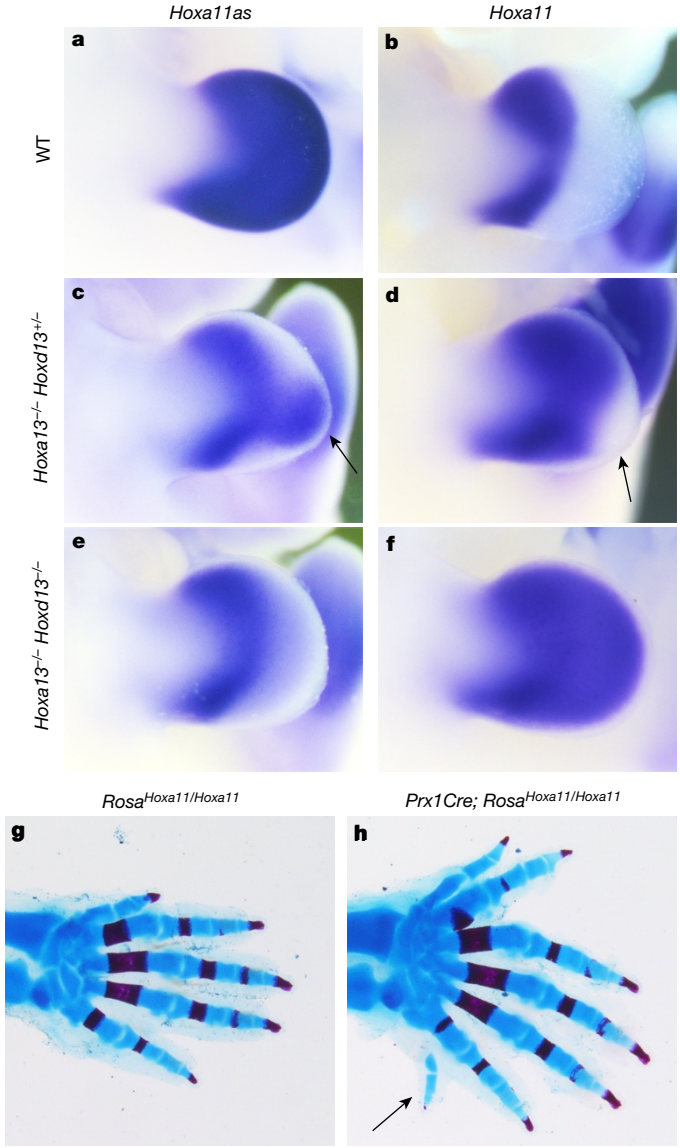

Figure 3 | *Hox13* inactivation disrupts *Hoxa11* antisense transcription in distal cells and distal *Hoxa11* expression results in the formation of supernumerary digits. a–f, *Hoxa11as* (probe A) (**a**, **c**, **e**) and *Hoxa11* (**b**, **d**, **f**) expression in E11.5 limb buds from wild-type (**a**, **b**), $Hoxa13^{-/-}$ $Hoxd13^{+/-}$ (**c**, **d**) and $Hoxa13^{-/-}$ $Hoxd13^{-/-}$ (**e**, **f**) mouse embryos. Arrows in **c** and **d** show the group of cells still expressing *Hoxa11as* in $Hoxa13^{-/-}$ $Hoxd13^{+/-}$ limbs (**c**), which corresponds to distal cells in which *Hoxa11* expression is not gained (**d**). **g**, **h**, Skeleton of $Rosa^{Hoxa11/Hoxa11}$ (**g**) and *Prx1Cre*; $Rosa^{Hoxa11/Hoxa11}$ (**h**) distal forelimb at postnatal day 0 (P0). Anterior is up. Original magnification, ×31.5 (**a**–**f**) and ×20 (**g**, **h**).

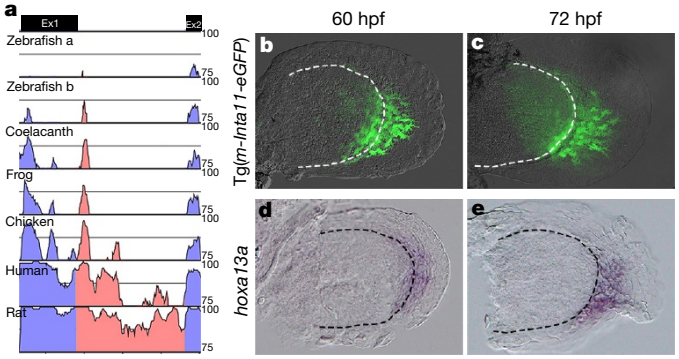

Figure 4 | The mouse *Hoxa11* antisense enhancer is functional in distal fins. a, mVISTA sequence conservation plot of the mouse *Hoxa11* intron (red) with tetrapod (rat, human, chicken and frog) and fish representatives (coelacanth and zebrafish). Ex1, exon 1; Ex2, exon 2. Note that zebrafish has two *hoxa11* genes expressed in developing fins, *hoxa11a* and *hoxa11b*. **b**, **c**, GFP expression in fin buds of Tg(*m-Inta11-eGFP*) transgenic zebrafish embryos at 60 hpf (**b**) and 72 hpf (**c**), revealing the enhancer activity of the mouse *Hoxa11* intron in fish. Note the filopodia-like protrusions in GFP^+ mesenchymal cells suggestive of a migration towards the fin fold. **d**, **e**, *hoxa13a* expression in developing fins at 60 hpf (**d**) and 72 hpf (**e**). Original magnification, ×400.

variations in the digit phenotype were observed among individuals, all homozygous mutants analysed were polydactylous (Extended Data Fig. 7c–e). Increased expression of *Hoxd11* in the presumptive autopod in the absence of *Hoxd13* also resulted in polydactyly, whereas a similar gain of *Hoxd10* or *Hoxd12* had no effect on digit number[27]. These data raise the possibility that the formation of extra digits upon ectopic expression of *Hoxa11* or *Hoxd11* distally reflects the divergence between *Hoxa11*/*Hoxd11* targets and those of the other 5′ *HoxA/D* genes. Notably, the evidence that *Hoxa11* expression in the distal limb results in the formation of extra digits indicates that the proximal restriction of *Hoxa11* expression is required for the pentadactyl state.

In contrast to the mutually exclusive *Hoxa11* and *Hoxa13* pattern in tetrapod limbs, *hoxa11* and *hoxa13* gene expression is largely overlapping in zebrafish fins[3–7] (Extended Data Fig. 8) as well as in other teleosts[28] (the medaka *Oryzias latipes*) and in fish models of both chondrichthyans[5] (*Scyliorhinus canicula*) and basal actinopterygians[3] (*Polyodon spathula*). The HOXA13/D13-mediated repression of *Hoxa11* identified in distal limb cells was thus probably implemented after the separation of actinopterygians and chondrichthyans, during the evolution of vertebrates towards tetrapod species. Consistent with this hypothesis, no *hoxa11* antisense transcription has been reported in fish[22,29] (Extended Data Fig. 9). Moreover, sequence comparison of the mouse *Hoxa11* intron showed robust conservation among tetrapods, whereas considerably weaker sequence conservation was observed with fish *hoxa11* orthologues (Fig. 4a). To examine whether the lack of *hoxa11* antisense transcription in fish could be due to the absence of a distal enhancer within *hoxa11* intron, we tested the zebrafish *hoxa11a* and *hoxa11b* intronic sequences for potential enhancer activity using transgenic reporter assays in both zebrafish and mice. Neither the *hoxa11a* nor *hoxa11b* intron was capable of triggering expression of a reporter gene in fin nor in mouse limb buds (Extended Data Table 1), indicating that there is no distal enhancer in *hoxa11a* nor *hoxa11b* intron. By contrast, when we tested the transcriptional activity of the mouse *Hoxa11* intron in zebrafish, the analysis of four stable transgenic lines revealed that the mouse *Hoxa11* intron was able to drive reporter gene expression in the pectoral fin mesenchyme (Fig. 4b, c). At 60 hours post-fertilization (hpf), eGFP-positive cells were present at the distal rim of the endoskeletal disc and migrating into the fin fold (Fig. 4b) and by 72 hpf most eGFP-positive cells were found in the fin fold mesenchyme (Fig. 4c). The expression of the reporter transgene was reminiscent of *hoxa13a* expression at 60 hpf (Fig. 4d) and 72 hpf (Fig. 4e), indicating that the mouse enhancer in *Hoxa11* intron was active in the *Hoxa13* domain also in zebrafish. Together, our data indicate that all the transcription factors required for the activity of the mouse enhancer are present in zebrafish fins, and that the enhancer driving *Hoxa11* antisense transcription does not exist in the intron of the zebrafish *hoxa11a* and *hoxa11b* genes. We therefore propose that the emergence of the enhancer triggering *Hoxa11* antisense transcription, and thus distal repression of *Hoxa11*, occurred in the course of evolution towards tetrapod species.

In summary, our work reveals that the mutually exclusive expression of *Hoxa11* and *Hoxa13* in tetrapods is associated with the emergence of a transcriptional enhancer in *Hoxa11* intron, which upon HOXA13/D13-dependent activation, triggers antisense transcription and thereby

prevents *Hoxa11* expression distally. On the basis of the evidence that this HOX13-mediated regulation of *Hoxa11* probably emerged during the fin-to-limb transition and the polydactyly resulting from distal expression of *Hoxa11* in mice, we propose that the evolution of *Hoxa11* regulation has contributed to the transition from polydactyly in stem-group (extinct) tetrapods to pentadactyly in extant tetrapods.

Online Content Methods, along with any additional Extended Data display items and Source Data, are available in the online version of the paper; references unique to these sections appear only in the online paper.

Received 10 April 2014; accepted 26 August 2016.
Published online 5 October 2016.

1. Shubin, N., Tabin, C. & Carroll, S. Deep homology and the origins of evolutionary novelty. *Nature* **457,** 818–823 (2009).
2. Coates, M. I., Jeffery, J. E. & Rut, M. Fins to limbs: what the fossils say. *Evol. Dev.* **4,** 390–401 (2002).
3. Davis, M. C., Dahn, R. D. & Shubin, N. H. An autopodial-like pattern of Hox expression in the fins of a basal actinopterygian fish. *Nature* **447,** 473–476 (2007).
4. Metscher, B. D. *et al.* Expression of Hoxa-11 and Hoxa-13 in the pectoral fin of a basal ray-finned fish, *Polyodon spathula*: implications for the origin of tetrapod limbs. *Evol. Dev.* **7,** 186–195 (2005).
5. Sakamoto, K. *et al.* Heterochronic shift in Hox-mediated activation of sonic hedgehog leads to morphological changes during fin development. *PLoS One* **4,** e5121 (2009).
6. Sordino, P., Duboule, D. & Kondo, T. Zebrafish *Hoxa* and *Evx-2* genes: cloning, developmental expression and implications for the functional evolution of posterior *Hox* genes. *Mech. Dev.* **59,** 165–175 (1996).
7. Ahn, D. & Ho, R. K. Tri-phasic expression of posterior *Hox* genes during development of pectoral fins in zebrafish: implications for the evolution of vertebrate paired appendages. *Dev. Biol.* **322,** 220–233 (2008).
8. Shubin, N., Tabin, C. & Carroll, S. Fossils, genes and the evolution of animal limbs. *Nature* **388,** 639–648 (1997).
9. Wagner, G. P. & Chiu, C. H. The tetrapod limb: a hypothesis on its origin. *J. Exp. Zool.* **291,** 226–240 (2001).
10. Sordino, P., van der Hoeven, F. & Duboule, D. *Hox* gene expression in teleost fins and the origin of vertebrate digits. *Nature* **375,** 678–681 (1995).
11. Freitas, R., Zhang, G. & Cohn, M. J. Biphasic *Hoxd* gene expression in shark paired fins reveals an ancient origin of the distal limb domain. *PLoS One* **2,** e754 (2007).
12. Freitas, R., Gómez-Marín, C., Wilson, J. M., Casares, F. & Gómez-Skarmeta, J. L. Hoxd13 contribution to the evolution of vertebrate appendages. *Dev. Cell* **23,** 1219–1229 (2012).
13. Woltering, J. M., Noordermeer, D., Leleu, M. & Duboule, D. Conservation and divergence of regulatory strategies at Hox loci and the origin of tetrapod digits. *PLoS Biol.* **12,** e1001773 (2014).
14. Fromental-Ramain, C. *et al.* Hoxa-13 and Hoxd-13 play a crucial role in the patterning of the limb autopod. *Development* **122,** 2997–3011 (1996).
15. Schneider, I. & Shubin, N. H. The origin of the tetrapod limb: from expeditions to enhancers. *Trends Genet.* **29,** 419–426 (2013).
16. Montavon, T. *et al.* A regulatory archipelago controls Hoix genes transcription in digits. *Cell* **147,** 1132–1145 (2011).
17. Berlivet, S. *et al.* Clustering of tissue-specific sub-TADs accompanies the regulation of *HoxA* genes in developing limbs. *PLoS Genet.* **9,** e1004018 (2013).
18. Gehrke, A. R. *et al.* Deep conservation of wrist and digit enhancers in fish. *Proc. Natl Acad. Sci. USA* **112,** 803–808 (2015).
19. Sheth, R., Bastida, M. F., Kmita, M. & Ros, M. "Self-regulation," a new facet of *Hox* genes' function. *Dev. Dyn.* **243,** 182–191 (2014).
20. Hsieh-Li, H. M. *et al.* Hoxa 11 structure, extensive antisense transcription, and function in male and female fertility. *Development* **121,** 1373–1385 (1995).
21. Potter, S. S. & Branford, W. W. Evolutionary conservation and tissue-specific processing of Hoxa 11 antisense transcripts. *Mamm. Genome* **9,** 799–806 (1998).
22. Leite-Castro, J., Beviano, V., Rodrigues, P. N., Freitas, R. & Hox, A. Genes and the fin-to-limb transition in vertebrates. *J. Dev. Biol*. **4,** 10 (2016).
23. Small, K. M. & Potter, S. S. Homeotic transformations and limb defects in *Hox A11* mutant mice. *Genes Dev*. **7,** 2318–2328 (1993).
24. Nelson, L. T., Rakshit, S., Sun, H. & Wellik, D. M. Generation and expression of a *Hoxa11eGFP* targeted allele in mice. *Dev. Dyn.* **237,** 3410–3416 (2008).
25. Scotti, M., Kherdjemil, Y., Roux, M. & Kmita, M. A *Hoxa13*:Cre mouse strain for conditional gene manipulation in developing limb, hindgut, and urogenital system. *Genesis* **53,** 366–376 (2015).
26. Logan, M. *et al.* Expression of Cre recombinase in the developing mouse limb bud driven by a *Prxl* enhancer. *Genesis* **33,** 77–80 (2002).
27. Kmita, M., Fraudeau, N., Hérault, Y. & Duboule, D. Serial deletions and duplications suggest a mechanism for the collinearity of *Hoxd* genes in limbs. *Nature* **420,** 145–150 (2002).
28. Takamatsu, N. *et al.* Duplicated *Abd-B* class genes in medaka *hoxAa* and *hoxAb* clusters exhibit differential expression patterns in pectoral fin buds. *Dev. Genes Evol.* **217,** 263–273 (2007).
29. Ulitsky, I., Shkumatava, A., Jan, C. H., Sive, H. & Bartel, D. P. Conserved function of lincRNAs in vertebrate embryonic development despite rapid sequence evolution. *Cell* **147,** 1537–1550 (2011).

Acknowledgements We thank Q. Zhu and L. Lian from the IRCM transgenic core facility for the ES cell work and production of transgenic mouse lines. We are particularly grateful to A. Kania for critical reading of the manuscript as well as laboratory members for insightful discussions and sharing reagents. This work was supported by the Canadian Institute for Health Research (MOP-115127) and the Canada Research Chair program to M.K. (RCHS0192), the Natural Sciences and Engineering Research Council of Canada (155817-2012) to M.-A.A. and Shriners Hospital Research grant 85400 to H.S.S. Y.K. was supported by a fellowship from the Molecular Biology program of the Université de Montréal and the IRCM fellowship Michel-Bélanger. R.S. was supported by a post-doctoral fellowship from the Canadian Institute for Health Research. D.M.W. and K.M.P. were supported by NIH NIAMS AR061402, with K.M.P. additionally supported by NIH T32 DE007057.

Author Contributions Y.K. and M.K. conceived the study and analysed the data. Y.K. designed and conducted all mouse experiments with the help of R.S. for the generation of the mouse lines. All fish experiments were performed by R.L.L. under the supervision of M.-A.A. R.S. performed the ChIP–seq experiments. A.D. provided technical help for the mouse experiments. G.M. performed preliminary experiments related to Figs 2a and 3c, e. D.M.W. and K.M.P provided *Hoxa11*$^{eGFP/eGFP}$ embryos. H.S.S. provided the HOXA13 and HOXD13 antibodies. M.K. wrote the paper. All authors commented on the manuscript.

Author Information Reprints and permissions information is available at www.nature.com/reprints. The authors declare no competing financial interests. Readers are welcome to comment on the online version of the paper. Correspondence and requests for materials should be addressed to M.K. (marie.kmita@ircm.qc.ca).

Reviewer Information *Nature* thanks R. Freitas, J. L. Gomez-Skarmeta and S. Mackem for their contribution to the peer review of this work.

METHODS

No statistical methods were used to predetermine sample size.

Mouse lines. *Hoxa11*^{Neo}, *Hoxa11*^{eGFP}, *Hoxa13null* (*Hoxa13*^{Str}) and *Hoxd13null* (*Hoxd13*^{lacZ}) mouse lines were previously described[14,23,24,30].

Rosa^{Hoxa11} knock-in allele was constructed as followed: PacI-AscI fragment from pBTG (Addgene plasmid 15037)[31] was inserted into the previously described *Rosa26* targeting vector[32] pROSA26Am1 (Addgene plasmid 15036)[31]. The mouse *Hoxa11* cDNA was inserted at the SmaI site within the MCS. The vector was linearized by SwaI digest prior electroporation into embryonic stem (ES) cells. After double selection using G418 and DTA negative selection, 96 ES cell clones were analysed by Southern blot for homologous recombination. Two independent clones were injected into blastocysts obtained from C57BL/6J mice, subsequently implanted into pseudo-pregnant females. After germline transmission of the *Rosa*^{Hoxa11} allele, mice and embryos were genotyped by Southern blot (a scheme with restriction sites and probes used is presented in Extended Data Fig. 6) and PCR. The following PCR primers were used: fw_wt : 5′-GCAATACCTTTCTGGGAGTTCT-3′, rev_wt : 5′-TCGGGTGAGCATGTCTTTTAATC-3′, rev_flox : 5′-TTCAATGGCC GATCCCATATT-3′, rev_del : 5′-AGGTTGGAGGAGTAGGAGTATG-3′. Wild-type band: 384 bp, flox band: 881 bp, del band: 583 bp. The moderate transcription resulting from the *Rosa26* promoter allowed for *Rosa26*^{Hoxa11} expression at a level comparable to the *Hoxa11* gain observed in our series of mutants.

Hoxa11$^{\Delta Int}$ mouse line was generated through pronuclei injection of single-guide RNAs (sgRNAs). We used the CRISPR (http://crispr.mit.edu/) platform to design sgRNAs flanking the region to delete. Complementary strands were annealed, phosphorylated and cloned into the BbsI site of pX330 CRISPR/Cas9 vector (Addgene plasmid 42230)[33]. SgInt1_fw : 5′-CACCGACTCCCCTTTCATAAAGCCC-3′; SgInt1_rev : 5′-AAACGCGCTTTATGAAAGGGGAGTC-3′; SgInt2_fw : 5′-CACCGAGCAACAGGCGAGTTTGCGC-3′; SgInt2_rev : 5′-AAACGCGC AAACTCGCCTGTTGCTC-3′. Mice and embryos were genotyped by Southern blot (a scheme with restriction sites and probe used is presented in Extended Data Fig. 2) as well as PCR. The Southern blot probe corresponds to the ScaI-HpaI fragment in the 3′ untranslated region (UTR) of the *Hoxa11* gene. Primers used for PCR genotyping, fw: 5′-GGCCACCTAAGGAAGGAGAG-3′; rev: 5′-GGCTCCGGTGCGTATAAAG-3′

Three *Prx1-Hoxa11as* transgenic lines were derived from three distinct founders obtained from pronuclear injection of the *Prx1-Hoxa11as* transgene. The *Prx1-Hoxa11as* transgene carries the *Prx1* promoter upstream of the mouse *Hoxa11as* (GenBank: U20367.1 and U20366.1) and the SV40 polyadenylation sequence was inserted downstream *Hoxa11as*. Embryos were genotyped by PCR using DNA from the amniotic membrane and the following pair of primers: fw: 5′-CTTTCTCTCTGGCTCTGATG-3′ and rev: 5′-GACAAGAACGCCGAGAA-3′ (for U20367.1) or fw: 5′-GTCCGAGGAAAAGGAGGTAG-3′ and rev: 5′-GCTCCTCTAACATGTATTTG-3′ (for U20366.1).

All mice were of mixed background (C57BL/6 X 129).

The Tg(*m-Inta11-LacZ*) transgene was generated by subcloning the mouse *Hoxa11* intron upstream of the *Hbb* (β-globin) minimal promoter and a LacZΔCpG NLS reporter. The *H19* insulator was inserted upstream of the *Hoxa11* intron. Tg(*m-Inta11-LacZ*) embryos were produced by pronuclear injection.

Whole-mount *in situ* hybridization, X-gal staining, skeletal preparations and imaging. For skeletal preparation, newborn mice were processed using the standard alcian blue alizarin red staining protocol[34] ($n = 10$ for each genotype).

Whole-mount *in situ* hybridizations were performed using previously described protocol[35] and probes[35] (*gfp*[36], *Neo*, *Hoxa11*, *Hoxa13*). Embryos were genotyped prior *in situ* hybridization (no blinding). *Hoxa11as* probes were generated using limb cDNA and the following primers: fw 5′-AGAGGCGCTGAGGAGCCTTCTC-3′ and rev 5′-GGCCGCTGTGGACACTAGCATATACC-3′ (probe A); fw 5′-CCT TCTCGGCGTTCTTGTC-3′ and rev 5′-GGCATACTCCTACTCCTCCAACCT-3′ (probe B).

X-gal staining was performed using standard protocol[35]. Embryos were genotyped after X-gal staining (which results in blinding test).

All mouse specimens were imaged using the Leica DFC450C camera. For each experiment, a minimum of three embryos per genotype was used as we considered that reproducible staining/expression patterns with three distinct embryos of the same genotype are significant. The experiments shown were repeated at least twice. We did not use the randomization method.

Subcloning of zebrafish *hoxa11a/b* intron and microinjections in zebrafish embryos. The zebrafish *hoxa11a* (713 bp; gene ID 58061, NCBI) and *hoxa11b* (747bp; gene ID 30382, NCBI) introns were amplified from zebrafish genomic DNA using the following primers: *hoxa11a* intron: fw 5′-GAATTCAACAGTAAG TACGAGCTCAAC-3′; rev 5′-GGTACCACCTAAATGTAAATACACGT-3′; *hoxa11b* intron: fw 5′-GAATTCCAGCGGCAGCAGCAGTACGT-3′; rev 5′-GGTACCCCGTGTCTTTTGTCCATCTAA-3′.

The zebrafish *hoxa11a* and *hoxa11b* and the mouse *Hoxa11* introns were subcloned into the pEGFP-N1 vector (CLONTECH Laboratories, Inc.) in which the CMV promoter upstream of eGFP was replaced with the human *HBB* minimal promoter using the following primers: fw 5′-GGATCCCTGGGCATAAAAGTCAG-3′, rev 5′-ACCGGTTCTGCTTCTGGAAGGCT-3′. This vector also contains the Tol2 arms to increase transgenesis efficiency. For screening purposes, a heart marker (*cmlc2:mCherry*[37]) was added to zebrafish Tg(*z-Inta11a-eGFP*) and Tg(*z-Inta11b-eGFP*) constructs. All constructs were microinjected in one-cell stage wild-type zebrafish embryos at a concentration of 100 ng μl^{-1} together with 50 ng μl^{-1} transposase mRNA.

Generation of zebrafish transgenic lines. Primary injected zebrafish (P_1) are raised until 3 months of age, and then are screened for transgenic progeny (F_1). P_1 fish are crossed with wild-type fish and the embryos are screened at 2 days post-fertilization (dpf). Owing to lack of fin fold eGFP expression in the Tg(*z-Inta11a-eGFP; cmlc2:mCherry*), Tg(*z-Inta11b-eGFP; cmlc2:mCherry*) injected fish, embryos were screened for the presence of the *cmlc2:mCherry* heart marker and genotyped to confirm the presence of the *hoxa11a/b intron:eGFP* elements. The following primers were used for genotyping: *hoxa11a*: fw 5′-GGTACCACCTAAATGTAAATACACGT-3′, rev (eGFP) 5′-GTCCTCCTTGAAGTCGATGC-3′; *hoxa11b*: fw 5′-GGTACCCC GTGTCTTTTGTCCATCTAA-3′, rev (eGFP) 5′-GTCCTCCTTGAAGTC GATGC-3′.

Three transgenic lines for Tg(*m-Inta11-eGFP*) were obtained to confirm the expression pattern. A fourth line containing the *cmlc2:mCherry* heart marker was also created. To confirm the *Hbb* minimal promoter does not drive tissue-specific expression alone, a transgenic line Tg(*HBB:eGFP; cmlc2:mCherry*) was also created and genotyped using the following primers: *Hbb*: fw 5′-GGATCCCTGGGCATAAAAGTCAG-3′, rev (eGFP) 5′-GTCCTCCTTGAAGTCGATGC-3′.

Zebrafish *in situ* hybridization. *In situ* hybridization on whole-mount embryos was performed as previously described[38]. Digoxigenin-labelled antisense RNA probes were generated using the following cDNAs: *hoxa13a* (500 bp; Addgene 36463), *hoxa13b* (700 bp; Addgene 36568), *hoxa11b* (probe 1 (Extended Data Fig. 8c, d); 800 bp; Addgene 36466). For *hoxa11a/b* antisense/sense RNA probes (Extended Data Fig. 9a, b), *hoxa11a* (713 bp; Gene ID 58061, NCBI) and *hoxa11b* (747 bp; gene ID 30382, NCBI) partial cDNAs (exon 1) were obtained by PCR with reverse transcription from total RNA of 24–48 hpf embryos using the following primers: *hoxa11a* exon 1: fw 5′-AT GATGGATTTTGACGAAAGGGTT-3′, rev 5′-TGTTCCCACCGCTAGTTTTT TCCT-3′; *hoxa11b* exon 1: fw 5′-ATGATGGATTTTGATGAGCGGGTA-3′, rev 5′-TGCTGCTGCCGCTGAATTTATCTT-3′.

For accurate comparison, *hoxa11a* and *hoxa11b* sense and antisense probes, respectively, are identical in length and were transcribed using the same RNA polymerase. *In situ* hybridizations were also performed in parallel with identical staining times.

Transfection and gene expression analysis. 293T cells (ATCC) were transfected using lipofactamine. Cells (800,000) were plated in 6-well plates. Cells were checked for mycoplasma contamination using Venor GeM Mycoplasma Detection Kit (MP0025 SIGMA). A total of 2 μg of DNA (250 ng reporter plasmid, 250 ng effector plasmid or empty expression vector), 25ng of mCherry expression vector as internal control and 1.45 μg carrier pBSK plasmid was used for each transfection. All transfections were performed in duplicates. Then, 24 h after transfection, the medium was changed and 48 h after transfection, cells were processed for RNA extraction. Reporter gene expression was normalized to internal control mCherry ($n = 3$). Gene expression (*Hoxa11*) was measured in dissected E11.5 forelimb buds of the *Rosa*^{Hoxa11} knock-in embryos that were stored in RNA later before RNA extraction ($n = 4$).

RNA extraction was done using RNAeasy Plus mini kit (Qiagen 74134). cDNA synthesis was performed using M-MuLV reverse transcriptase (NEB) and a mix of random primers and oligo-dT on 1ug of total RNA. Quantitative real-time-PCR was performed with cDNA and the SYBR Green kit (applied biosystems) using the following primers: fw 5′-AGGAGAAGGAGCGACGG-3′ and rev 5′-GGTATTTGGTATAAGGGCAGCG-3′ (*Hoxa11*); fw 5′-CTTT GTCAAGCTCATTTCCTGG-3′ and rev 5′-TCTTGCTCAGTGTCCTTGC-3′ (*Gapdh*); fw 5′-TTGACCTAAAGACCATTGCACTTC-3′ and rev 5′-TTCTCA TGATGACTGCAGCAAA-3′ (*Tbp*); fw 5′-GCCTACAACGTCAACATCAAG-3′ and rev 5′-GCGTTCGTACTGTTCCAC-3′ (mCherry); fw 5′-GACCCTGA AGTTCATCTGCA-3′ and rev 5′-CCGTCGTCCTTGAAGAAGA-3′ (*gfp*).

Study approval. All mice experiments described in this article were approved by the Animal Care Commitee of the Institut de Recherches Cliniques de Montréal (protocols 2011-39 and 2014-14) and zebrafish experiments were approved by uOttawa Animal Care Committee (protocol BL-2317-R1).

30. Kmita, M., Kondo, T. & Duboule, D. Targeted inversion of a polar silencer within the HoxD complex re-allocates domains of enhancer sharing. *Nat. Genet.* **26,** 451–454 (2000).
31. Murtaugh, L. C., Stanger, B. Z., Kwan, K. M. & Melton, D. A. Notch signaling controls multiple steps of pancreatic differentiation. *Proc. Natl Acad. Sci. USA* **100,** 14920–14925 (2003).
32. Soriano, P. Generalized *lacZ* expression with the ROSA26 Cre reporter strain. *Nat. Genet.* **21,** 70–71 (1999).
33. Cong, L. *et al.* Multiplex genome engineering using CRISPR/Cas systems. *Science* **339,** 819–823 (2013).
34. Sheth, R. *et al. Hox* genes regulate digit patterning by controlling the wavelength of a Turing-type mechanism. *Science* **338,** 1476–1480 (2012).
35. Scotti, M. & Kmita, M. Recruitment of 5′ *Hoxa* genes in the allantois is essential for proper extra-embryonic function in placental mammals. *Development* **139,** 731–739 (2012).
36. Mattar, P. *et al.* Basic helix-loop-helix transcription factors cooperate to specify a cortical projection neuron identity. *Mol. Cell. Biol.* **28,** 1456–1469 (2008).
37. Yelon, D., Horne, S. A. & Stainier, D. Y. Restricted expression of cardiac myosin genes reveals regulated aspects of heart tube assembly in zebrafish. *Dev. Biol.* **214,** 23–37 (1999).
38. Thisse, C. & Thisse, B. High-resolution in situ hybridization to whole-mount zebrafish embryos. *Nat. Protocols* **3,** 59–69 (2008).

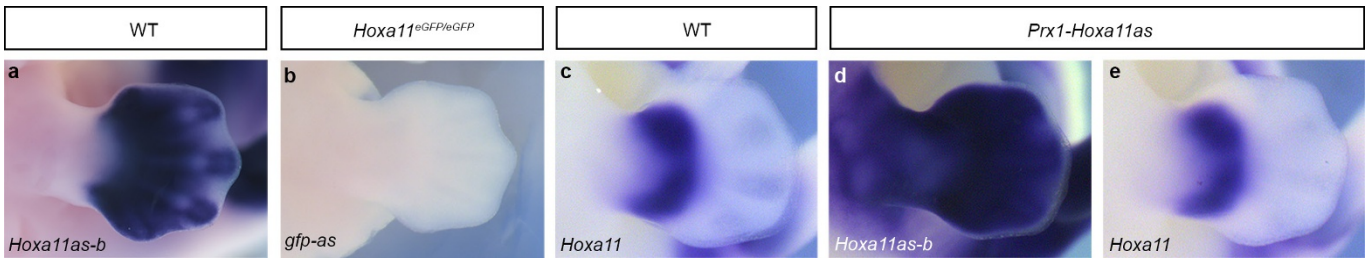

Extended Data Figure 1 | Absence of antisense transcription 3′ to the *Hoxa11* promoter in the *Hoxa11*$^{eGFP/eGFP}$ limb and evidence that *Hoxa11as-b* transcripts produced in *trans* have no effect on *Hoxa11* expression. a, **b**, Detection of *Hoxa11as-b* transcripts in wild-type limb buds at E12.5 (**a**), and whole-mount *in situ* hybridization to detect *gfp* antisense transcripts in *Hoxa11*$^{eGFP/eGFP}$ limb buds at E12.5 (**b**). **c**–**e**, *Hoxa11* expression in wild-type limb buds (**c**), and *Hoxa11as-b* (**d**) and *Hoxa11* (**e**) expression in *Prx1-Hoxa11as* limb buds. Original magnification, ×31.5.

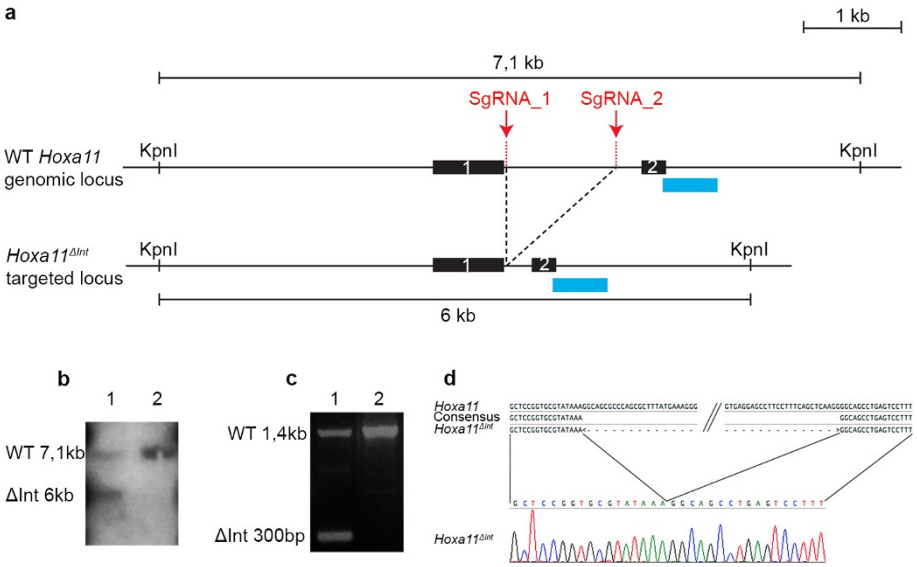

Extended Data Figure 2 | Deletion of the distal enhancer in *Hoxa11* intron using CRISPR-Cas9. a, Scheme of the wild-type and targeted (*Hoxa11*$^{\Delta Int}$) loci. Sites targeted by the single-guide RNAs (sgRNA_1 and sgRNA_2) for the CRISPR-Cas9-mediated deletion of the distal enhancer. The blue rectangles indicate the position of the DNA probe used to confirm the deletion by Southern blot in **b**. **b**, Lane 1 shows the 6-kb KpnI band resulting from the CRISPR-Cas9-mediated deletion. Lane 2 was loaded with wild-type DNA. **c**, PCR reaction using a forward primer located upstream of sgRNA_1 and a reverse primer located downstream sgRNA_2 shows the presence of a 300 bp (ΔInt 300 bp) fragment expected for the *Hoxa11*$^{\Delta Int}$ allele. **d**, The sequence of the 300-bp PCR fragment confirms the CRISPR-Cas9-mediated deletion of the *Hoxa11* intronic region containing the distal enhancer (only the sequence encompassing the deletion breakpoints is shown).

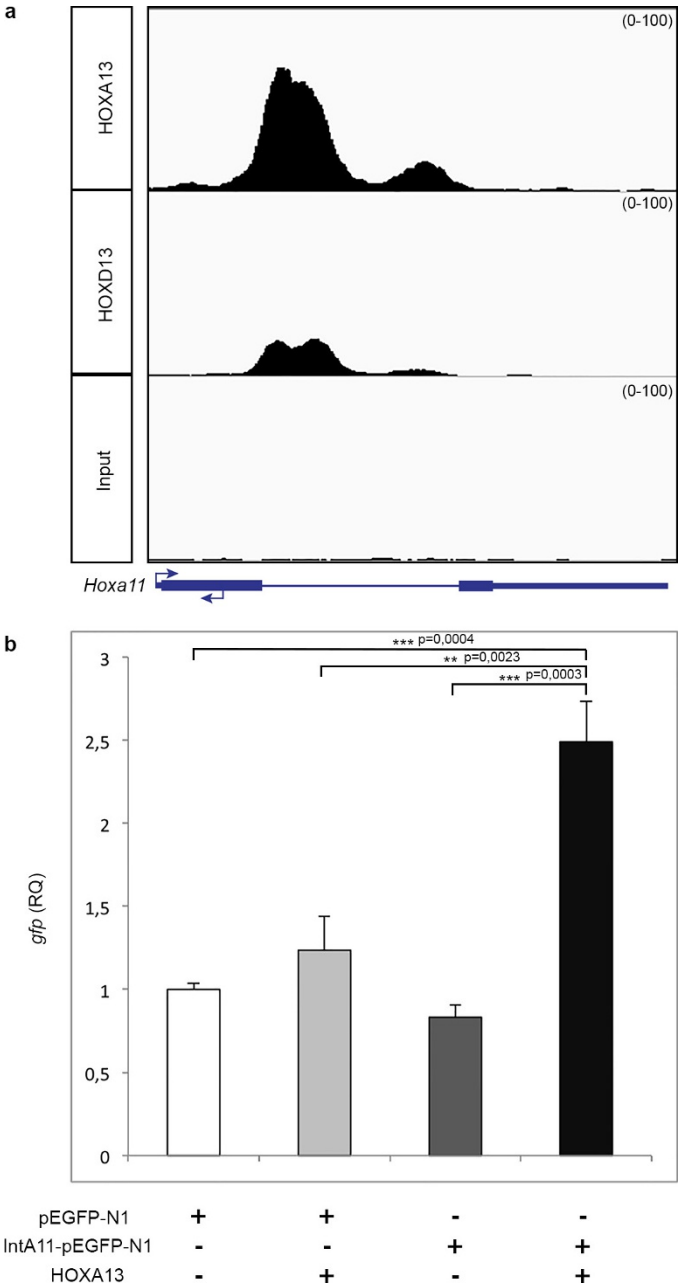

Extended Data Figure 3 | The distal enhancer located in the *Hoxa11* intron is bound by HOXA13 and HOXD13 in distal limb cells and its activity is increased by HOXA13 in 293T cells. a, Integrative genomics viewer (IGV) screenshot showing HOXA13 and HOXD13 ChIP–seq data at the *Hoxa11* locus. These ChIP–seq data were obtained using chromatin from distal forelimb buds of wild-type E11.5 mouse embryos (R. Sheth *et al.*, manuscript submitted). **b**, Transfection assay shows HOXA13 dependent activation of *Hoxa11* intron driving reporter gene expression. Two-tailed Tukey's multiple comparisons test was performed. Error bars indicate s.d ($n = 3$). RQ, relative quantification.

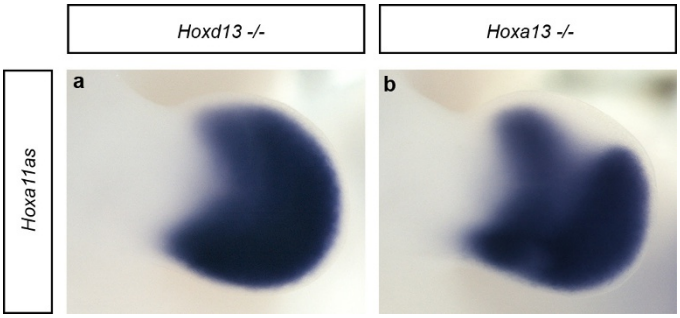

Extended Data Figure 4 | Individual inactivation of *Hoxa13* or *Hoxd13* is not sufficient to fully abrogate antisense transcription in distal limbs. **a**, **b**, Whole-mount *in situ* hybridization, using probe A (see Fig. 1) to detect all antisense transcripts, on *Hoxd13*$^{-/-}$ (**a**) and *Hoxa13*$^{-/-}$ (**b**) mouse limb buds at E11.5. Antisense transcription in distal limbs remains robust in both mutants but a clear reduction is seen in the distal *Hoxa13*$^{-/-}$ limbs. Original magnification, ×31.5.

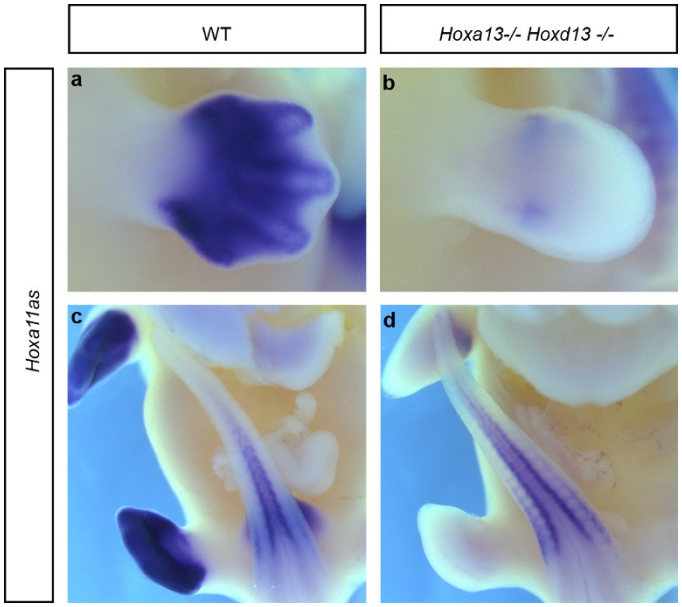

Extended Data Figure 5 | Inactivation of both *Hoxa13* and *Hoxd13* disrupts antisense transcription overlapping with the *Hoxa11* exon 1. **a**–**d**, *Hoxa11as-b* expression (probe B in Fig. 1) in limb buds (**a**, **b**) and tail buds (**c**, **d**) from wild-type (**a**, **c**) and $Hoxa13^{-/-}$ $Hoxd13^{-/-}$ (**b**, **d**) E12.5 mouse embryos. Whole-mount *in situ* hybridization shows that *Hoxa11as-b* expression in tail buds (internal control) is similar in both the wild-type (**c**) and double-mutant (**d**) embryos, whereas there is almost no expression remaining in $Hoxa13^{-/-}$ $Hoxd13^{-/-}$ limb buds (**b**). Original magnification, ×31.5.

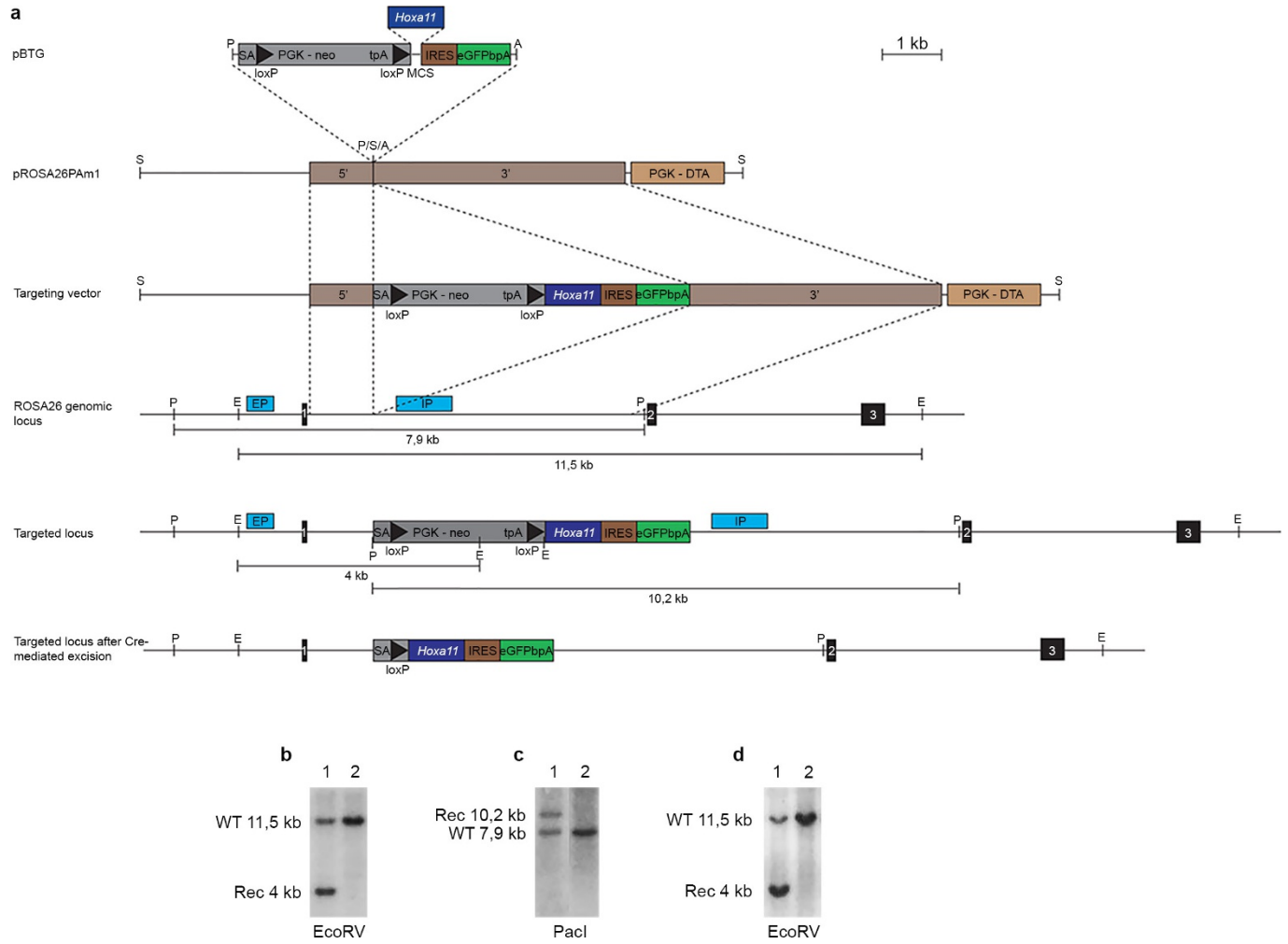

Extended Data Figure 6 | Generation of the *Rosa*^{Hoxa11} knock-in mouse line. a, Targeting of the endogenous *Rosa26* locus (top three lines). The wild-type *Rosa26* locus is shown below (middle). Regions used as homologous arms for the recombination in ES cells are indicated by brown rectangles labelled 5′ and 3′, respectively. Scheme of the targeted locus after homologous recombination in ES cells and after Cre-mediated recombination is shown at the bottom. The position of the internal (IP) and external (EP) probes and restriction sites used for Southern blot analysis are indicated on both the wild-type and targeted locus. **b**, **c**, Southern blots of ES cells clones using the internal probe (**b**) and external probe (**c**) to detect the targeted allele (lane 1). **d**, Southern blot of wild-type (lane 2) and heterozygous (lane 1) mice. A, AscI; E, EcoRV; P, PacI; S, SwaI.

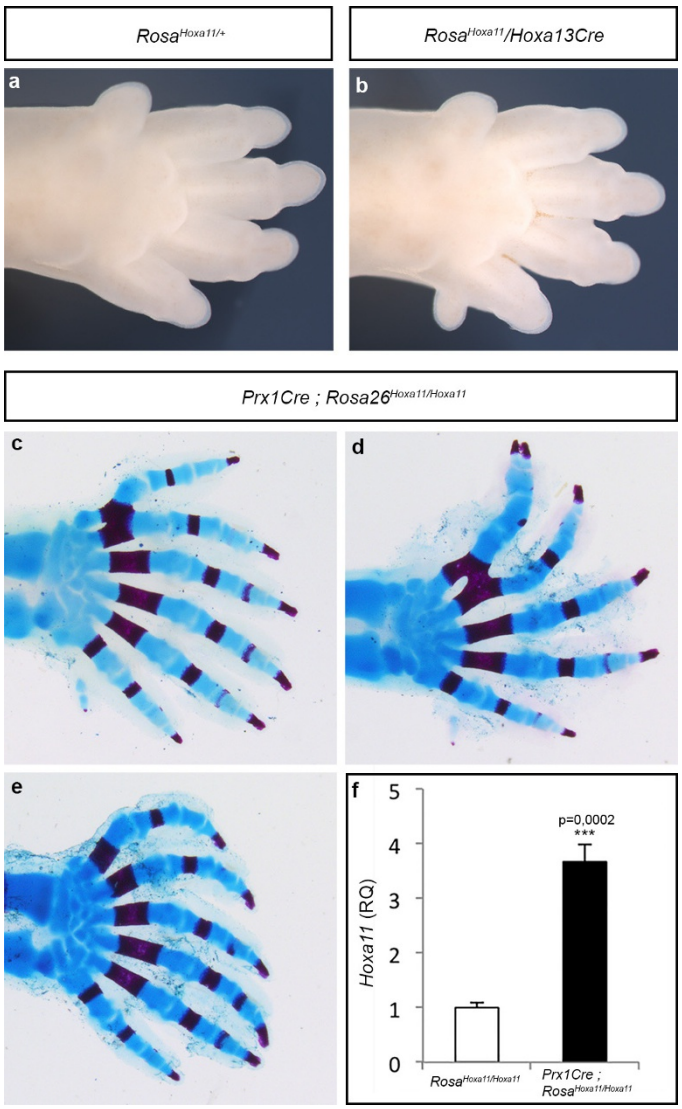

Extended Data Figure 7 | The conditional gain of *Hoxa11* using the *Hoxa13Cre* allele results in the formation of supernumerary digits. **a**, **b**, Autopod of *Rosa*$^{Hoxa11/+}$ (**a**) and *Rosa*^{Hoxa11} *Hoxa13Cre* (**b**) at E15.5. Anterior is up. The *Rosa26* locus and *Hoxa13Cre* allele being on the same chromosome (Chr6), the gain-of-function phenotype was assessed with only one copy of the *Rosa*^{Hoxa11} allele. **c**–**e**, Autopod skeletons of *Prx1Cre*; *Rosa*$^{Hoxa11/Hoxa11}$ mice at P0 from four distinct mutants (anterior is up). The number of digits varies from 6 to 7, with often a small post-axial extra-digit (posterior). The extra-digit phenotype is fully penetrant upon Cre-activation of two copies of the *Rosa*^{Hoxa11} allele ($n = 10$). Original magnification, ×20.**d**, Quantification of *Hoxa11* expression level by quantitative reverse transcriptase PCR (RT–qPCR) on RNA extracted from E11.5 forelimb, relative to both *Gapdh* and *Tbp* mRNA of *Prx1Cre*; *Rosa*$^{Hoxa11/Hoxa11}$ embryos. Two-tailed *t*-test was performed. Error bars indicate s.d ($n = 4$).

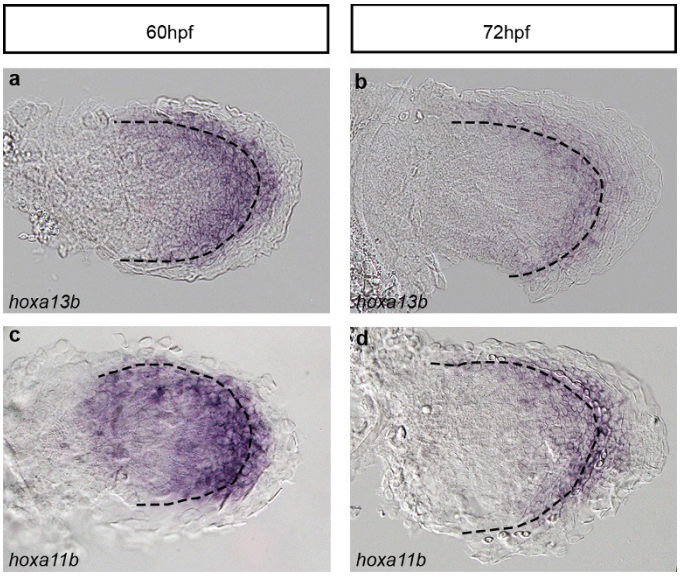

Extended Data Figure 8 | *hoxa11* and *hoxa13* are expressed in overlapping domains in zebrafish fins. a–d, Expression of *hoxa13b* (**a**, **b**) and *hoxa11b* (**c**, **d**) in zebrafish fins at 60 hpf (**a**, **c**) and 72 hpf (**b**, **d**). Dotted lines indicate the boundary between the endochondral disc and the fin fold. Original magnification, ×400.

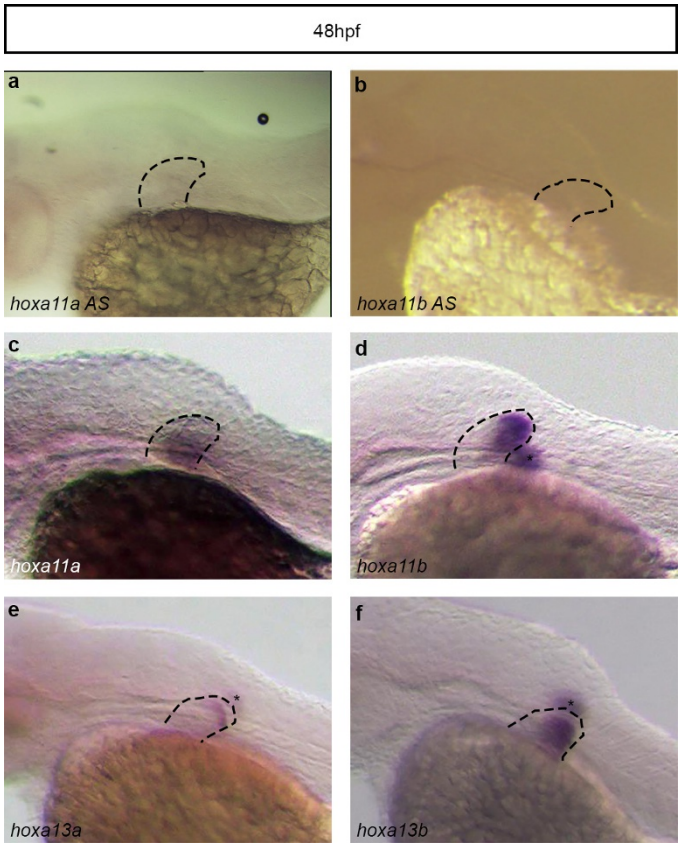

Extended Data Figure 9 | Absence of antisense transcription at the *hoxa11a* and *hoxa11b* loci in zebrafish fins. a, **b**, Whole-mount *in situ* hybridization with probes designed to detect putative antisense transcription at *hoxa11a* (**a**) and *hoxa11b* (**b**). **c**–**f**, No antisense transcription is detected, whereas expression of *hoxa11a* (**c**), *hoxa11b* (**d**), *hoxa13a* (**e**) and *hoxa13b* (**f**) is observed in zebrafish fins at the same stage. Asterisks correspond to the staining from the fin on the other side of the embryo. Original magnification, ×63.

Extended Data Table 1 | Summary of transient transgenic embryos analysed

Zebrafish Transient Transgenics	
Construct	% of eGFP positive fish
Tg(*HBB:eGFP*)	0% (n=74)
Tg(*z-Inta11a-eGFP*)	0% (n=105)
Tg(*z-Inta11b-eGFP*)	1.19% (n=84)
Tg(*m-Inia11-eGFP*)	91.9% (n=123)
Tg(*HBB:eGFP; cmlc2:mCherry*)	1.25% (n=94)
Tg(*z-Inta11a-eGFP; cmlc2:mCherry*)	0% (n=200)
Tg(*z-Inta11b-eGFP; cmlc2:mCherry*)	0% (n=300)
Tg(*m-Inia11-eGFP; cmlc2:mCherry*)	88.9% (n=53)
Mouse Transient Transgenics	
Construct	% of eGFP positive embryos (# eGFP positive / # genotyped positive)
Tg(*z-Inta11a-eGFP*)	0% (n=0/10)
Tg(*z-Inta11b-eGFP*)	0% (n=0/7)

Zebrafish stable lines for Tg(*z-Inta11a-eGFP; cmlc2:mCherry*); Tg(*z-Inta11b-eGFP; cmlc2:mCherry*) were also generated and three genotyped F_1 embryos per line were analysed and confirmed for the absence of *gfp* expression. For Tg(*m-Inta11-eGFP; cmlc2:mCherry*), four distinct transgenic lines were also generated and analysed.